Friction **11**(3): 369–382 (2023)
https://doi.org/10.1007/s40544-022-0597-6
ISSN 2223-7690
CN 10-1237/TH

RESEARCH ARTICLE

Two-dimensional molybdenum carbide (MXene) as an efficient nanoadditive for achieving superlubricity under ultrahigh pressure

Shuang YI[1,2], Yitong GUO[3], Jinjin LI[1,*], Yuxin ZHANG[2], Aiguo ZHOU[3], Jianbin LUO[1]

[1] *State Key Laboratory of Tribology, Tsinghua University, Beijing 100084, China*

[2] *College of Materials Science and Engineering, Chongqing University, Chongqing 400044, China*

[3] *Henan Key Laboratory of Materials on Deep-Earth Engineering, Henan Polytechnic University, Jiaozuo 454003, China*

Received: 29 October 2021 / Revised: 26 November 2021 / Accepted: 08 January 2022

Abstract: In this study, a robust macroscale liquid superlubricity with a coefficient of friction of 0.004 was achieved by introducing molybdenum carbide (Mo_2CT_x) MXene nanoparticles as lubricating additives in a lithium hexafluorophosphate-based ionic liquid at Si_3N_4–sapphire interfaces. The maximal contact pressure in the superlubricity state could reach 1.42 GPa, which far exceeds the limit of the superlubricity regime in previous studies. The results indicate that a composite tribofilm (mainly containing molybdenum oxide and phosphorus oxide) that formed at the interface by a tribochemical reaction contributed to the excellent antiwear performance. Furthermore, the extremely low shear strength of the tribofilm and the interlayers of Mo_2CT_x MXene contributed to the superlubricity. This work demonstrates the promising potential of Mo_2CT_x MXene in improving superlubricity properties, which could accelerate the application of superlubricity in mechanical systems.

Keywords: molybdenum carbide (Mo_2CT_x) MXene; superlubricity; additives; ultrahigh pressure; wear resistance

1 Introduction

Friction and wear cause significant energy loss on a mechanical surface, serious material loss, shortened service life, and increased safety accidents involving machinery [1, 2]. Therefore, many researchers have used various methods to reduce friction and wear [3]. In this context, a new concept of superlubricity, with a coefficient of friction (COF) of less than 0.01, was proposed to enhance lubrication performance at the nanoscale or macroscale, which could provide ultralow friction and wear to reduce energy loss. Currently, different superlubricity approaches exist, such as solid, liquid, and solid–liquid coupling superlubricity systems. For solid superlubricity, molybdenum disulfide (MoS_2) [4], graphite sheets [5], the graphene family of materials [6, 7], and diamond-like carbon [8, 9] could act as typical solid superlubricity materials at the nanoscale or macroscale.

Compared with solid superlubricity, liquid superlubricity is more efficiently realized at the macroscale with lubrication by various liquids, such as phosphoric acid [10], ionic liquid (IL) [11], oleic acid [12], polyalphaolefin oil [13], and biological liquid [14]. To enhance the load capacity and antiwear ability in the liquid superlubricity state, conventional layered materials, including black phosphorus [15], graphene materials [7, 16], hexagonal boron nitride [17], and layered double hydroxides [18], have been used as lubricant additives because of their extremely low shear strength in their interlayers. These layered materials have a similar two-dimensional (2D) layered structure, which can be adsorbed on the worn-out zone after the friction process to reduce wear and

* Corresponding author: Jinjin LI, E-mail: lijinjin@mail.tsinghua.edu.cn

simultaneously provide extremely low shear strength between friction pairs. However, one limitation of these liquid materials, related to the contact pressure (dividing the normal load by the contact area), must be improved. With lubrication by these liquids, even though the initial contact pressure between the frictional pairs is high (on the order of gigapascals), the final contact pressure during the superlubricity period is still at a much lower order of magnitude. This is caused by the severe wear occurring during the running-in period.

Recently, a novel member of the 2D layered material family, MXene, was formed by a few atoms with thick layers of transition metal carbides, nitrides, or carbon nitride based on MAX-phases [19–21]. This material exhibits excellent electrochemistry, thermoelectricity, lubrication, and other properties, making it suitable for use in energy storage [22], catalysis [23], lubrication [24], etc. Some studies on the MXene lubrication have been reported [25, 26]. For example, in a number of studies, Ti_3C_2 MXene or its composite materials were used as solid coatings to enhance wear resistance and tribological properties [27–32]. Other researchers have investigated MXene nanoparticles as lubricant additives that can reduce friction and wear [33–35]. Although previous research on the MXene lubrication has revealed that MXene has the potential to achieve low friction and wear, industry requirements (ultralow friction and ultrahigh contact pressure) still hinder the application of MXene. In this study, Mo_2CT_x MXene nanoparticles were synthesized and introduced into lithium hexafluorophosphate-based IL as a nanoadditive. Robust macroscale superlubricity has been achieved under an ultrahigh contact pressure of as much as 1.42 GPa, which is a 136.67% increase compared with previous results in Ref. [36]. The lubricating behavior related to this liquid superlubricity under ultrahigh pressure using Mo_2CT_x MXene as a lubricating nanoadditive was studied, and the related mechanism was revealed.

2 Experimental

2.1 MXene and lubricant synthesis

The precursor Mo_2Ga_2C powders were synthesized from gallium ingots (Ga, 99.99 wt%, Beijing Xingrongyuan Co., Ltd., China) and molybdenum carbide powders (Mo_2C, 99.5 wt%, 325 mesh, Sigma Aldrich Co., Ltd., USA). Mo_2C and Ga were weighed in a molar ratio of 1:5 [37, 38]. Subsequently, the resulting Mo_2Ga_2C powders were added to 40 mL of etching solution. The etching solution was prepared by mixing 2.0 g of LiF (99.9 wt%, Aladdin Industrial Co., Ltd., China) and 6-M HCl (11.8 mol/L, Shuangshuang Chemical Reagent Co., Ltd., China). Afterward, the mixture was washed until a pH of approximately 6.0 by using deionized water to obtain Mo_2CT_x MXene particles. Thereafter, the collected Mo_2CT_x MXene particles were mixed with deionized water at a ratio of 0.2–5 mg/mL to prepare an aqueous solution of Mo_2CT_x MXene and sonicated for 48 h. The IL formed *in situ* was synthesized by dissolving 0.1 g of $LiPF_6$ (purity of 97%, Aladdin Industrial Co., Ltd., China) in 2 g of ethylene glycol (EG) (purity of 99%, Aladdin Industrial Co., Ltd., China) via sonication for 8 h, followed by magnetic stirring at 50 °C for 8 h (Fig. 1(d)). Once the IL was prepared, it was immediately mixed with a Mo_2CT_x MXene aqueous solution at a ratio of 1:5 by weight, and the mixtures were denoted as Mo_2CT_x–IL (Fig. 1(e)). The concentration of nanoparticles varied from 0.021 to 0.416 wt%. For comparison, the graphene oxide (GO)–IL and MoS_2–IL solutions were prepared with the same volume concentration as that of Mo_2CT_x–IL.

2.2 Material characterization

The dried Mo_2CT_x MXene particles were tested by the atomic force microscope (Icon, Bruker, Germany) to measure the sizes of the Mo_2CT_x MXene nanoparticles. The crystal structures of the Mo_2CT_x MXene nanoparticles were detected using the X-ray diffractometer (XRD) (Bruker, Germany) with 2θ ranging from 5° to 65°. The morphology of the Mo_2CT_x MXene nanoparticles was analyzed by the high-resolution transmission electron microscope (HRTEM) (2100F, JEM, Japan). The original chemical composition of the Mo_2CT_x MXene nanoparticles was characterized by the X-ray photoelectron spectroscope (XPS) (PHI Quantera II, Japan). The chemical groups of Mo_2CT_x MXene and IL were detected by the Fourier transform infrared spectroscope (FTIR) (Vertex 70V, Bruker, Germany) and the Raman spectroscope (HR-800, Horiba, Japan),

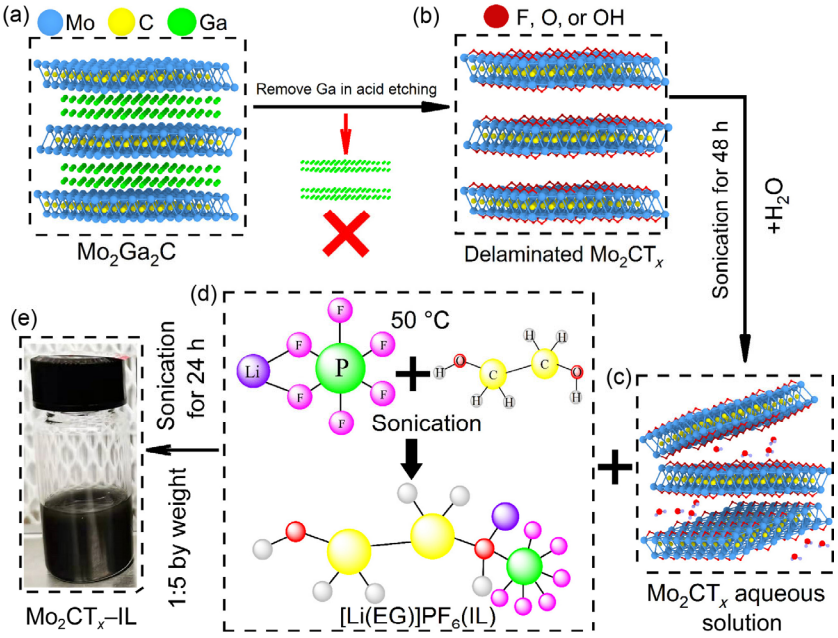

Fig. 1 (a–c) Preparation of Mo_2CT_x MXene aqueous solution and schematic structure of Mo_2CT_x MXene, where the blue, yellow, and green orbs represent molybdenum, carbon, and gallium atoms, respectively, and the red orbs are the functional groups of fluorine, oxygen, or hydroxyl functional-containing groups. (d) Preparation of IL by dissolving lithium hexafluorophosphate (0.1 g) in ethylene glycol (2 g) via 8 h of sonication at 50 °C. (e) Preparation of Mo_2CT_x–IL solution by mixing IL and Mo_2CT_x aqueous solution with a mass ratio of 1:5 via 24 h of sonication.

respectively. The average size of the Mo_2CT_x MXene was measured using a commercial zeta potential instrument (Zetasizer Nano Series, Malvern, UK).

2.3 Tribological test

Friction and wear tests were conducted using a universal micro-tribotester in a ball-on-disk mode (UMT-5, Bruker, USA). A fixed Si_3N_4 ball was loaded onto a rotatable sapphire disk. Subsequently, 20 μL of the lubricant was dripped onto the contact surfaces in each test. The applied load of the ball varied from 1 to 6 N, corresponding to the initial contact pressures of 1.31–2.40 GPa at the interface. The sliding speed of the disk ranged from 0.004 to 0.375 m/s. All tests were conducted at a room temperature of 25 °C and a relative humidity of 20%–25%.

2.4 Surface characterization

The diameter of the wear scar and the roughness of the worn-out zone on the ball and plate were observed using a 3D white-light interferometer (Nexview, ZYGO Lambda, USA). The topographies of the worn zones were acquired by the scanning electron microscope (SEM) (Quanta 200 FEG, FEI, USA). The wear zones on the surfaces were analyzed using the XPS and Raman spectroscopy after the friction test. The cross-sectional structures of the worn zones on the surfaces were observed using HRTEM.

3 Results and discussion

3.1 Mo_2CT_x MXene characterization

Mo_2CT_x MXene was synthesized by etching Ga from Mo_2Ga_2C powders using etchants, and subsequently delaminated by sonication in water (Fig. 1). The Mo_2CT_x–IL solution was prepared by mixing a lithium hexafluorophosphate-based IL and a Mo_2CT_x MXene aqueous solution with a mass ratio of 1:5. After the synthesis of Mo_2CT_x MXene, the morphology of Mo_2CT_x MXene was first observed using SEM (Fig. 2(a)), which showed a highly crystalline structure of Mo_2CT_x MXene nanoparticles.

The lattice structures of Mo_2CT_x MXene were investigated by XRD, as shown in Fig. 2(b), showing the first peak at $2\theta = 8.6°$, which was smaller than that of the precursor Mo_2Ga_2C [39]. This is an indication

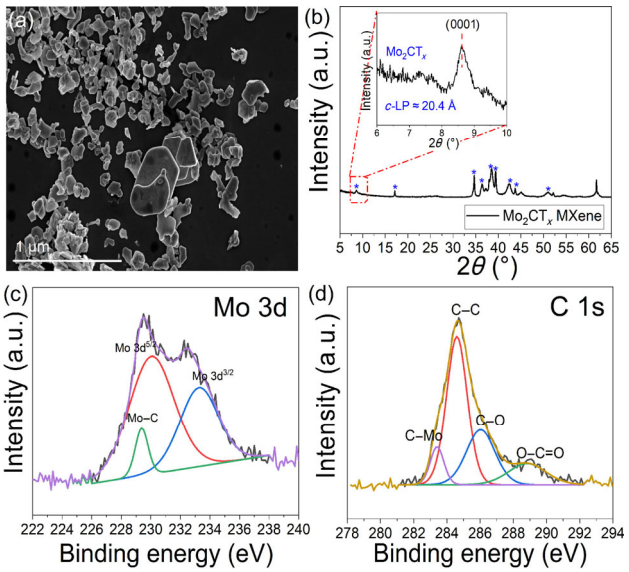

Fig. 2 (a) SEM image of Mo_2CT_x MXene nanoparticles, (b) XRD pattern of Mo_2CT_x MXene, (c) XPS spectra of Mo 3d of the original Mo_2CT_x MXene, and (d) XPS spectra of C 1s of the original Mo_2CT_x MXene.

of the successful removal of the gallium layers. The peak at 8.6° was indicative of the typical MAX to MXene transformation, and the (0001) peak broadened and shifted to a lower angle because of an increase in the *c*-lattice parameter (*c*-LP) from 18.1 to 20.4 Å [39–41]. The high-resolution XPS spectra of Mo 3d and C 1s of the original Mo_2CT_x MXene are shown in Figs. 2(c) and 2(d), respectively. For the Mo 3d, there were three main peaks located at 229.8, 230.8, and 233.1 eV. The peaks were assigned to Mo–C, Mo $3d^{5/2}$, and Mo $3d^{3/2}$ [42], respectively. For C 1s, four main peaks were located at 283.2, 284.6, 286.1, and 289.3 eV. These peaks were assigned to C–Mo, C–C, C–O, and O–C=O bonds, respectively. FTIR was used to detect the reciprocities between IL and Mo_2CT_x (Fig. S1(a) in the Electronic Supplementary Material (ESM)). The peaks at 1,087 and 1,109 cm^{-1} proved the existence of C–O bonds, and the peak at 1,642 cm^{-1} proved the presence of Mo. Furthermore, the peaks at 2,875 and 2,938 cm^{-1} indicated the existence of C–H, and the peak at 3,305 cm^{-1} indicated the existence of hydroxyl groups [43]. The peaks in the Raman spectra located at 488 and 546 cm^{-1} are the standard peaks of Mo_2CT_x MXene (Fig. S1(b) in the ESM), confirming the successful preparation of the Mo_2CT_x MXene. The size distribution of Mo_2CT_x MXene in IL was measured using a Zetasizer, which showed that the MXene in IL had an average size of 531 nm (Fig. S1(c) in the ESM).

3.2 Tribological performances

To estimate the macroscale tribological properties of Mo_2CT_x–IL, the friction experiments were performed at the Si_3N_4–sapphire interface with lubrication by IL, Mo_2CT_x aqueous solution, and Mo_2CT_x–IL, respectively, under a load of 3 N and a sliding speed of 0.1 m/s (Fig. 3(a)). The results showed that the COF first displayed an unstable oscillation in the range of 0.08–0.1 from 0 to 1,200 s with lubrication by the Mo_2CT_x MXene aqueous solution. Subsequently, the COF started a sudden drop from 0.1 to 0.058. However, this declining tendency of the COF was not maintained for a long time, and it started to rise after 1,500 s. This performance indicates that the Mo_2CT_x nanoparticles can reduce friction, but they cannot result in an ultralow COF. Thereafter, the IL (without MXene) as a lubricant was tested, showing a robust state with a COF of approximately 0.05 in the entire friction test. This phenomenon indicates that IL has good stability as a lubricant, but it still cannot achieve superlubricity. Based on these results, Mo_2CT_x MXene nanoparticles were selected as lubricating nanoadditives to be introduced into the IL, and the COF of the Mo_2CT_x–IL solution showed a similar tendency to that of Mo_2CT_x during the initial period of 900 s. Subsequently, the COF gradually dropped from 0.09 to 0.005 during the period of 900–1,350 s, which entered the superlubricity regime. Finally, the COF maintained stably at 0.004, and it could be sustained for at least 4.5 h (Fig. 3(b)), corresponding to a sliding distance of 1,620 m.

After the friction test, the wear scar and surface roughness on the Si_3N_4 and sapphire surfaces were characterized using 3D white-light interferometry. The results showed that the diameters of the wear scar on the Si_3N_4 surface were 55.46 and 91.2 μm after lubrication by Mo_2CT_x–IL and IL, respectively. The corresponding widths of the wear tracks on the sapphire surface were 59.6 and 105.3 μm, respectively (Fig. S2 in the ESM). The average contact pressures (dividing the normal load by the contact area) after lubrication by Mo_2CT_x–IL and IL were 1.24 GPa and 459.48 MPa, respectively. Compared with lubrication by IL, the contact pressure directly increased by 170.46% with lubrication by Mo_2CT_x–IL, indicating that the Mo_2CT_x

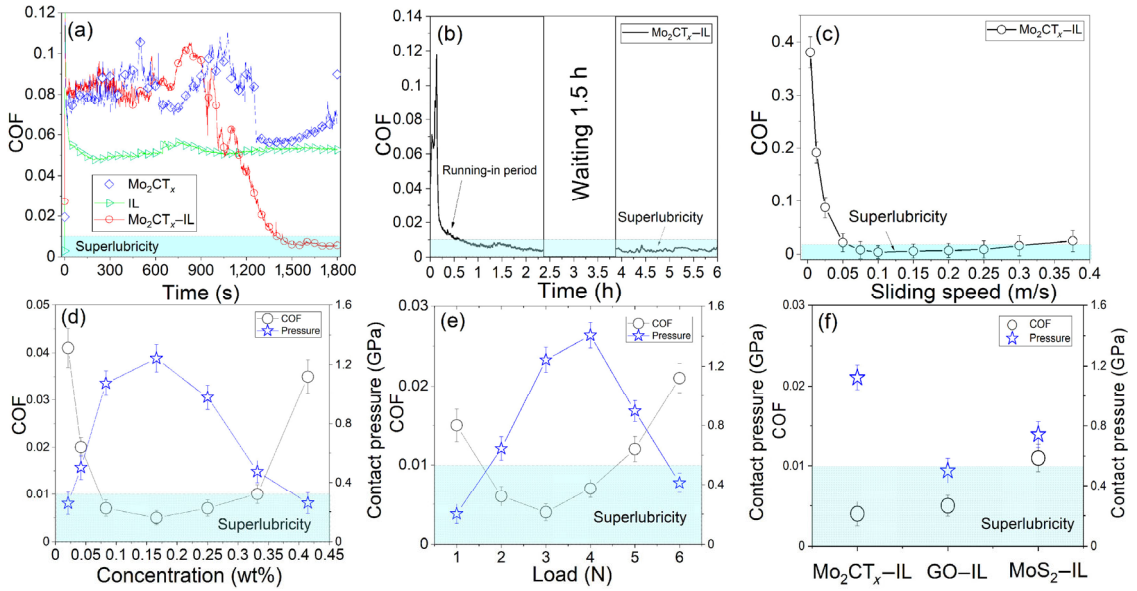

Fig. 3 (a) COF vs. time with lubrication by IL, Mo_2CT_x aqueous solution, and Mo_2CT_x–IL with a load of 3 N and a sliding speed of 0.1 m/s. (b) COF for long-run testing (up to 4.5 h) with lubrication by Mo_2CT_x–IL. (c) Influence of sliding speed on COF during the superlubricity period with a normal load of 3 N. The concentration of Mo_2CT_x in IL is 0.166 wt%. (d) COFs and corresponding contact pressures during the superlubricity period with lubrication by various concentrations of Mo_2CT_x–IL with a normal load of 3 N and a sliding speed of 0.1 m/s. (e) COFs and corresponding contact pressures during the superlubricity period under different normal loads (1–6 N) with a concentration of 0.166 wt% and a sliding speed of 0.1 m/s. (f) COFs and corresponding contact pressures during the superlubricity period with different solutions, including Mo_2CT_x–IL, GO–IL, and MoS_2–IL with the same volume concentration as Mo_2CT_x–IL. The normal load is 3 N, and the sliding speed is 0.1 m/s.

MXene nanoparticles as additives in IL could reduce friction and suppress wear to enhance the contact pressure. Generally, a high contact pressure is detrimental to the achievement of superlubricity. However, the introduction of Mo_2CT_x MXene additives in ILs could make the contact pressure of superlubricity exceed 1 GPa, which is far higher than that achieved by elastohydrodynamic lubrication (< 300 MPa) [44]. Meanwhile, the surface roughness of the wear scar on the Si_3N_4 surface after lubrication by Mo_2CT_x–IL was 23.2 nm, which was significantly smaller than that with lubrication by IL (56.4 nm). The corresponding surface roughnesses of the wear tracks on the sapphire surface were 18.9 and 33.4 nm with lubrication by Mo_2CT_x–IL and IL, respectively.

An additional investigation of the influence of the sliding speed on COF was performed with lubrication by Mo_2CT_x MXene nanoparticles as additives in the IL (Fig. 3(c)). The COF decreased from 0.37 to 0.018 when the sliding speed increased from 0.004 to 0.05 m/s, which was noticeably in the non-superlubricity regime. Subsequently, the COF decreased to 0.004 when the sliding speed further increased to 0.075 m/s, which entered the superlubricity regime. This was followed by maintaining the superlubricity state (the COF varied slightly from 0.004 to 0.008) when the sliding speed increased from 0.075 to 0.25 m/s. When the sliding speed exceeded 0.3 m/s, the COF was greater than 0.01, which was indicative of the failure of the superlubricity state. The evolution of the COF with sliding speed was consistent with the Stribeck curve, indicating that the hydrodynamic effect may also influence the superlubricity state. When the sliding speed was extremely low, the hydrodynamic effect was weak, leading to an increase in the COF. This illustrates that there is an optimal range of sliding speeds in which a robust superlubricity state can be achieved with lubrication by Mo_2CT_x–IL.

Subsequently, a friction test was carried out with lubrication using different concentrations of Mo_2CT_x MXene as lubricating additives (from 0.021 to 0.416 wt%) in IL (Fig. 3(d)). The extremely low concentration (< 0.042 wt%) clearly cannot lead to the achievement of superlubricity. The COF decreased from 0.042 to 0.021 when the concentration of Mo_2CT_x MXene increased from 0.021 to 0.042 wt%. However, when the

concentration of Mo_2CT_x MXene reached 0.083 wt%, the COF decreased to 0.007, which entered the superlubricity regime. When the concentration of Mo_2CT_x–IL further increased from 0.083 to 0.332 wt%, the results showed that the COF first decreased slightly from 0.008 to 0.004 when the concentration of Mo_2CT_x MXene reached 0.166 wt%, and then it had a slight increase (the COFs were always less than 0.01). However, when the Mo_2CT_x MXene concentration reached 0.416 wt%, the superlubricity state was damaged with a high COF of 0.035. Moreover, the lubrication state became unstable with a violent fluctuation of the COF (Fig. S3 in the ESM). These results indicate that the COF was significantly influenced by the concentration of Mo_2CT_x MXene, and an optimal concentration range (0.083–0.332 wt%) was necessary to achieve the superlubricity state. The diameter and wear volume of the wear scar on the Si_3N_4 surface were also measured after the friction test (Figs. S4 and S5 in the ESM), showing that suitable concentrations of 0.083–0.25 wt% of Mo_2CT_x could also suppress the surface wear and meanwhile achieve the superlubricity state, which leads to a high contact pressure (> 900 MPa) for superlubricity. The maximum contact pressure in the superlubricity state could reach 1.24 GPa with a concentration of 0.166 wt% (Fig. 3(d)). However, when the concentration was too low or too high, superlubricity could not be achieved, and there was also severe wear (corresponding to a low contact pressure). This is because there were not enough Mo_2CT_x nanoparticles to enter the contact zone when the concentration was extremely low, and the agglomeration of the Mo_2CT_x nanoparticles occurred when the concentration was very high, both of which were harmful for achieving superlubricity and reducing surface wear.

Next, the influence of the normal load on the COF with lubrication by the 0.166 wt% of Mo_2CT_x MXene as additives in IL was investigated (Fig. 3(e)). When a normal load of 1 N was applied, the final COF decreased to 0.015, which belongs to the non-superlubricity regime. After the normal load was increased to 2 N, the COF directly dropped to 0.006, which entered the superlubricity regime. The lowest average value of the COF, 0.004, was achieved by further increasing the normal load to 3 N. However, when the normal load exceeded 3 N, the COF gradually increased with increasing load and finally reached 0.021 at a normal load of 6 N. These results indicate that the optimal normal load range is 2–4 N, in which superlubricity can be achieved with Mo_2CT_x–IL. When the load was too low or too high, superlubricity could not be achieved, which may be because the tribofilms could not be completely formed with an extremely low load, and the tribofilms were damaged with a very high load. Compared with the corresponding contact pressures after the friction test, high contact pressures (> 900 MPa) could be achieved when the normal load was in the range of 3–5 N, and the maximal contact pressure for superlubricity could reach 1.42 GPa at a normal load of 4 N (Fig. S6 in the ESM).

To verify the excellent lubrication performance of the Mo_2CT_x–IL, two other typical 2D materials (GO and MoS_2) were selected and mixed with IL at the same volume concentration of Mo_2CT_x, referred to as GO–IL and MoS_2–IL, respectively. The COF results in Fig. 3(f) were taken as the average values in the stable period, showing that a COF of 0.005 could be achieved by using GO–IL as a lubricant, while the COF would increase to 0.011 by using MoS_2–IL as a lubricant. The corresponding wear scars after lubrication by GO–IL and MoS_2–IL were 82.74 and 71.8 μm, respectively (Fig. S7 in the ESM), corresponding the contact pressures of 558.23 and 741.31 MPa, respectively. Although the GO–IL could achieve superlubricity, the wear scar was much larger than those of Mo_2CT_x–IL and MoS_2–IL, corresponding to a significantly lower contact pressure. This result confirms that molybdenum has much better antiwear ability than graphene.

3.3 Analysis of wear interface

After the friction test, the worn-out zone on the Si_3N_4 surface was examined using SEM (Fig. 4(a)). Some adsorbed substances can be observed on the Si_3N_4 surface in the worn-out zone after lubrication by Mo_2CT_x–IL. To analyze the composition of this area, energy-dispersive X-ray spectroscopy (EDS) mapping was performed in the worn-out zone (Figs. 4(b) and 4(c)). Mo and P were detected on the Si_3N_4 surface based on the strong contrast signals in the EDS diagram. The wear track on the sapphire surface was

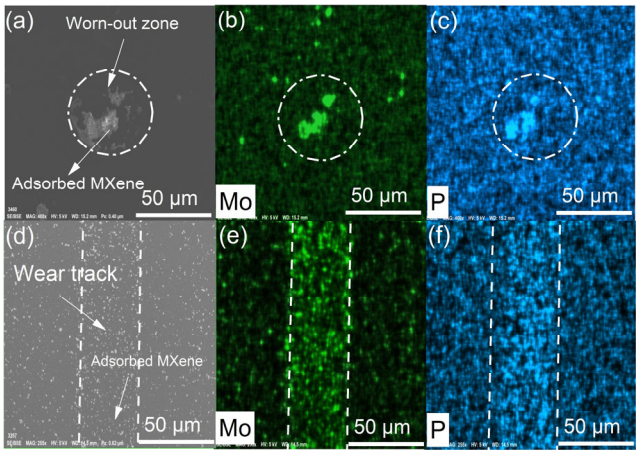

Fig. 4 Analyses of the wear scar on the Si_3N_4 and sapphire surface after lubrication by Mo_2CT_x–IL with a normal load of 3 N and a sliding speed of 0.1 m/s. (a) SEM image of morphology on the Si_3N_4 surface. (b, c) EDS elemental mapping of the worn-out zone on the Si_3N_4 surface. The elements are Mo and P, respectively. (d) SEM image of morphology on the sapphire surface. (e, f) EDS elemental mapping of the worn-out zone on the sapphire surface. The elements are Mo and P, respectively.

also examined using SEM with EDS (Figs. 4(d)–4(f)), in which adsorbed nanoparticles were observed in the wear track. The EDS results also showed a strong contrast in the Mo and P elements in the wear track. According to these results, it can be inferred that there may be Mo_2CT_x MXene nanoparticles and IL molecules adsorbed in the worn-out zone through physical adsorption or tribochemical reaction during the friction test.

To determine the change in chemical composition on the friction surfaces and possible tribochemical reaction in the friction process, the worn-out zones on the Si_3N_4 and sapphire surfaces after lubrication by Mo_2CT_x–IL were also characterized by XPS (Fig. 5 and Fig. S8 in the ESM). On the worn-out surface of the Si_3N_4, the main element of C 1s contained four main peaks located at 283.0, 284.8, 286.6, and 288.4 eV (Fig. 5(a)), corresponding to C–Mo, carbon in aliphatic chains (C–C), C–O, and O–C=O bonds, respectively. The detected C–O bond may be derived from the IL or oxidation of the Mo_2CT_x MXene nanoparticles. The existence of the C–Mo and O–C=O bonds mainly originated from the Mo_2CT_x MXene (Fig. 2(d)), proving that there were Mo_2CT_x nanoparticles adsorbed on the Si_3N_4 surface. For the Mo element (Fig. 5(b)), there were four main peaks located at 228.6, 230.0, 232.1, and 234.4 eV. These peaks were assigned to Mo–O, Mo–C, Mo $3d^{5/2}$, and Mo $3d^{3/2}$, respectively. In comparison with the original XPS results of Mo_2CT_x MXene in Fig. 2(c), the existence of the Mo–O bond

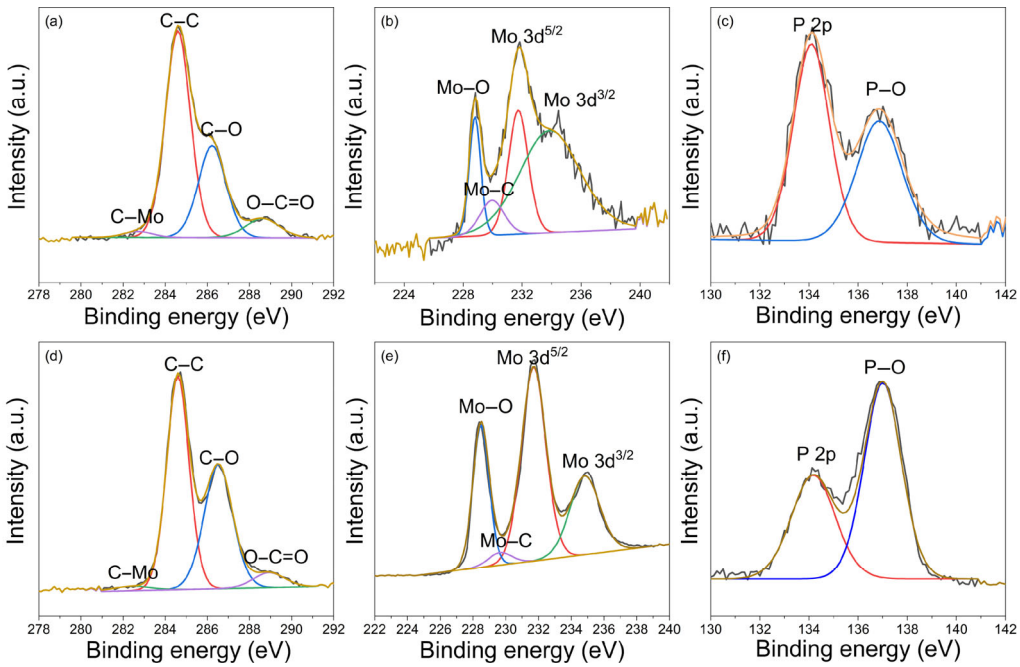

Fig. 5 XPS spectra of basic chemical elements on the worn-out zone of Si_3N_4 and sapphire surfaces after lubrication by Mo_2CT_x–IL. (a–c) C 1s, Mo 3d, and P 2p on the worn-out zone of the Si_3N_4 ball, respectively; (d–f) C 1s, Mo 3d, and P 2p on the worn-out zone of the sapphire surface, respectively.

showed that some Mo_2CT_x MXene participated in the oxidation reaction and produced molybdenum oxides (Mo_xO_y) in the tribofilm. The production of Mo_xO_y improved the antiwear ability due to the molybdenum oxide, which is a wear-resistant material [45, 46]. For the P 2p, strong peaks were located at 134.5 and 137.3 eV (Fig. 5(c)), which were assigned to P 2p and P–O bonds, respectively. This indicates that phosphorus oxides (P_xO_y) were produced on the worn-out surface of Si_3N_4. There were also two peaks of F 1s located at 684.6 and 687.8 eV (Fig. S8(a) in the ESM), which corresponded to fluorides and C–F bonds, respectively [47]. This result was consistent with Ref. [11], in which the anion of PF_6^- in IL was transformed into fluorides and phosphates by friction. For the Si 2p, Si–N (99.5 eV) and Si–O (101.7 eV) bonds were detected (Fig. S8(b) in the ESM), and the existence of the Si–O bond indicates the presence of a tribochemical reaction between Si_3N_4 and water, leading to the formation of a silica layer.

At the same time, a worn-out zone was also detected by XPS on sapphire after lubrication by Mo_2CT_x–IL, and it displayed peaks similar to those of the Si_3N_4 surface (Figs. 5(d)–5(f)). The C 1s contained four main peaks located at 282.9 eV (C–Mo), 284.8 eV (C–C), 286.6 eV (C–O), and 288.4 eV (O–C=O), as shown in Fig. 5(d). The detected Mo–O and P–O bonds confirm the production of Mo_xO_y and P_xO_y in the tribofilm on the sapphire surface by a tribochemical reaction. In addition, there were two F 1s peaks located at 684.2 and 685.9 eV on the sapphire surface (Fig. S8(c) in the ESM), which arose from the fluorides and AlF_6^{3-}, respectively. The XPS results of Al 2p also prove the generation of Al–F bonds, indicating a tribochemical reaction between Al_2O_3 and PF_6^- anions (Fig. S8(d) in the ESM). Combining these XPS results and the EDS mapping in Fig. 4 indicates that there were tribofilms formed in the worn-out zone on the Si_3N_4 and sapphire surfaces, which were mainly composed of Mo_xO_y, P_xO_y, and fluorides.

To reveal the structure of the tribofilm further, cross-sectional layers of the worn-out zone on the Si_3N_4 and sapphire surfaces were prepared using a focused ion beam after lubrication with Mo_2CT_x–IL (the sampling regions are marked in Fig. S9 in the ESM). HRTEM was then conducted on the cross-sectional samples of the tribofilm in the contact zone (Fig. 6). The thickness of the tribofilm on the Si_3N_4 surface was approximately 45.6 nm (Fig. 6(a)). Furthermore, EDS in line scan mode was performed to analyze the elemental distribution and determine the composition of the tribofilm (Fig. 6(c)). Along with the elemental distributions of P, Mo, and O, the production of P_xO_y and Mo_xO_y occurred in the tribofilm with approximate thicknesses of 25 and 20 nm, respectively. The formation of Mo_xO_y and P_xO_y confirms that the tribochemical reaction occurred for the Mo_2CT_x MXene nanoparticles and IL on the Si_3N_4 surface, in accordance with the XPS results in Fig. 5. There was an overlapping region for Mo_xO_y and P_xO_y production, indicating that the tribofilm had a composite structure.

Figure 6(c) shows that the Si_3N_4 surface also participated in the tribochemical reaction ($Si_3N_4 + 6H_2O \rightarrow 3SiO_2 + 4NH_3$), leading to the formation of silica on the Si_3N_4 surface with an approximate thickness of 12 nm. Additionally, the structure of Mo_2CT_x MXene in the tribofilm was clearly observed in the enlarged HRTEM image (area A in Fig. 6(e)), which showed a multilayer structure with an interlayer spacing of approximately 0.7 nm. The detected layers of Mo_2CT_x MXene were parallel to the sliding direction, which had a beneficial effect on providing low shear strength. Raman detection was performed on the worn-out zone after the friction test (Fig. S10 in the ESM), and the Raman spectra of the worn-out zone of the Si_3N_4 surface (Fig. S10(a) in the ESM) exhibited the same bands as the original Raman results in Fig. S1(b) in the ESM, further demonstrating that Mo_2CT_x MXene nanoparticles were adsorbed on the worn-out zone of the Si_3N_4 surface.

On the sapphire surface, a tribofilm with a thickness of 57.2 nm was also observed (Fig. 6(b)). The EDS results show that Mo_xO_y and P_xO_y were produced in the tribofilm on the sapphire surface with thicknesses of 31 and 30 nm, respectively (Fig. 6(d)). The higher-magnification HRTEM image (area B) displayed some layer structures with an interlayer spacing of 0.57–0.65 nm in the tribofilm, which corresponded to the Mo_2CT_x nanoparticles. The inherent thickness of Mo_2C is approximately 5 Å [39], and the increase in the interlayer spacing is caused by surface termination or possible intercalated species. The Raman results also prove that the Mo_2CT_x MXene nanoparticles were

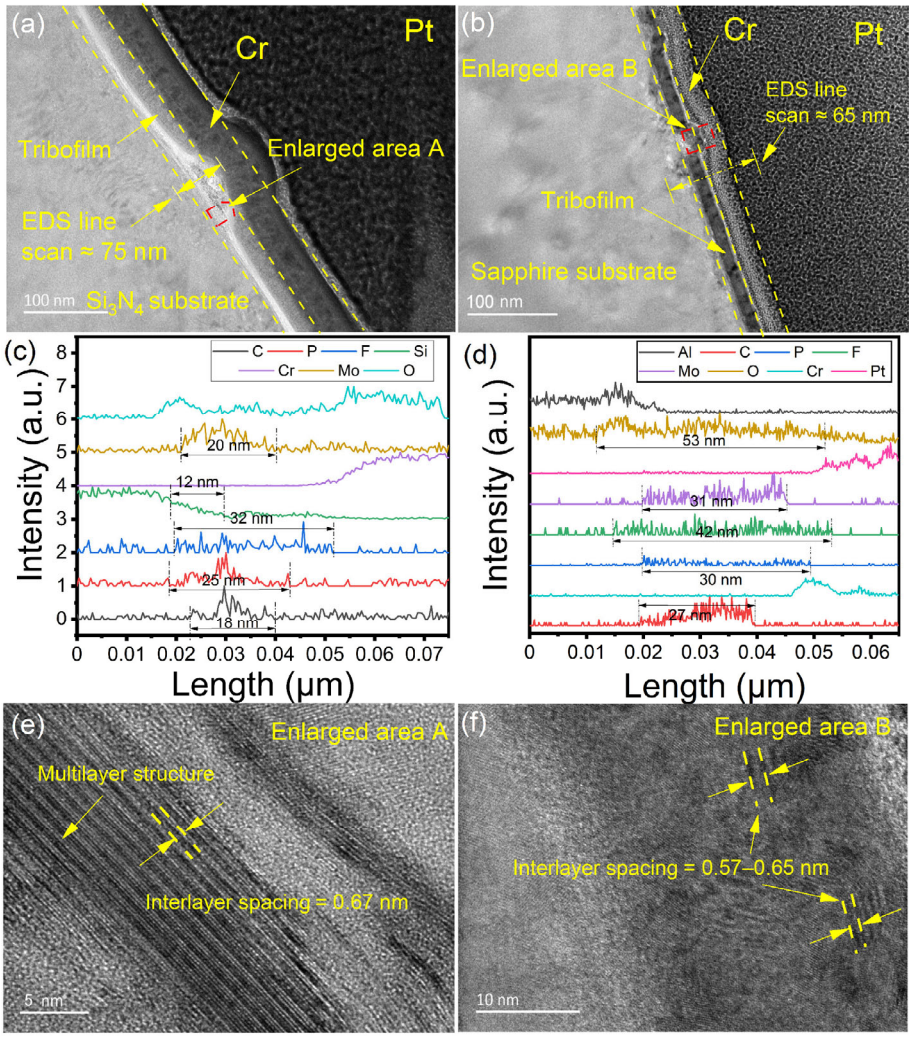

Fig. 6 Cross-sectional structure of the tribofilm on the friction surface after friction test: (a) HRTEM images of the tribofilm formed on the Si_3N_4 surface; (b) HRTEM images of the tribofilm formed on the sapphire surface; (c) elemental distributions of Si, P, O, Mo, F, Cr, and C along the cross-sectional profile in the enlarged area of Fig. 6(a) on the Si_3N_4 surface; (d) elemental distributions of Al, C, P, F, Mo, O, Cr, and Pt along the cross-sectional profile in the enlarged area of Fig. 6(b) on the sapphire surface; (e) enlarged view of HRTEM image of the tribofilm (area A) formed on the Si_3N_4 surface; and (f) enlarged view of HRTEM image of the tribofilm (area B) formed on the sapphire surface.

adsorbed on the sapphire surface (Fig. S10(b) in the ESM).

3.4 Mechanism of ultrahigh contact pressure under superlubricity

According to previous studies, it is difficult to achieve superlubricity under a contact pressure of more than 600 MPa (in the absence of coatings). However, in this work, the extended pressure limit of superlubricity was on the order of gigapascals. This implies a specific lubrication mechanism rather than the traditional elastohydrodynamic lubrication when the Mo_2CT_x MXene nanoparticles were used as lubricant additives, which was beneficial for achieving superlubricity under ultrahigh pressures. To determine the lubrication regime in the superlubricity state, the thickness (h_c) of the lubricating film at the Si_3N_4–sapphire interface was estimated using the Hamrock–Dowson formula [48]. The calculation in Section S12 in the ESM showed that the liquid film thickness in the superlubricity state was in the range of 41.95–45.67 nm (45.67 nm for 2 N, 43.42 nm for 3 N, and 41.95 nm for 4 N, respectively). The ratio of the liquid film thickness to the equivalent roughness of the two worn-out zones

(λ) was used to classify the lubrication regime, which was calculated using the equation of $\lambda = \frac{h}{\sqrt{\sigma_1^2 + \sigma_2^2}}$, where σ is the surface roughness (23.2 nm for balls and 18.9 nm for the plate). The calculation yields λ = 1.41–1.52, which implies that the lubrication regime was located in the mixed lubrication regime (containing the boundary and elastohydrodynamic lubrication).

For the running-in period, the COF oscillated unsteadily at 0.09, and slight wear occurred on the Si_3N_4 and sapphire surfaces with lubrication by Mo_2CT_x–IL. Although the COF value was larger than that with IL lubrication during the running-in period, the wear was significantly lower than that with IL lubrication. This phenomenon demonstrates that Mo_2CT_x MXene nanoparticles play a dominant role in the inhibition of wear during the running-in period. It is speculated that the Mo_2CT_x MXene nanoparticles are adsorbed in the worn-out zone of the friction pairs from the beginning of the friction test, which can prevent direct contact between the Si_3N_4 and sapphire surface. To confirm that the Mo_2CT_x MXene nanoparticles were adsorbed on the friction surfaces within a very short period, XPS was performed on the contact zone of the Si_3N_4 surface after lubrication by Mo_2CT_x–IL for running-in periods of 1 and 3 min. The XPS results show a strong Mo 3d and C 1s signal in the contact zone of the Si_3N_4 surface (Fig. S11 in the ESM), which are typical peaks of Mo_2CT_x MXene nanoparticles (Figs. 2(c) and 2(d)). These results illustrate the excellent adsorption of Mo_2CT_x MXene nanoparticles from the beginning of the friction test, which prevented the friction pairs from direct contact and thereby suppressed surface wear. Furthermore, the existence of the Mo–O bond during the running-in period indicates that Mo_2CT_x–IL participated in the tribochemical reaction from the beginning of the test. A protective film containing Mo_xO_y formed, which could further decrease abrasion owing to the excellent antiwear property of Mo_xO_y [49]. Compared with other 2D materials, such as GO and MoS_2, Mo_2CT_x MXene nanoparticles exhibited a much better reduction in wear (Fig. S7 in the ESM). Therefore, the antiwear properties of Mo_2CT_x MXene nanoparticles do not only depend on its layer structure, but also are related on the antiwear properties of the Mo_2CT_x MXene nanoparticles themselves, which are not presented in the traditional 2D materials, such as GO and MoS_2. After the running-in period was complete, the COF was directly reduced from 0.09 to 0.004, entering the superlubricity regime.

During the superlubricity period, the lubrication state entered the mixed lubrication regime. A composite structure of tribofilms containing Mo_xO_y, P_xO_y, silica, and fluorides was formed on the friction surfaces by tribochemical reactions, which can provide extremely low shear strength for the boundary lubrication. Here, the ultralow shear strength occurred for three main reasons. First, Mo_xO_y and P_xO_y containing –OH groups are favorable for combining with water [50, 51]; thus, a water layer can form through double hydrogen bonding between the –OH groups and water molecules, which could reduce the shear strength of the tribofilm. Second, the silica colloid layer could promote the boundary lubrication because it was an excellent boundary lubricating material in a water environment [52], which could further reduce the shear strength of the tribofilm. Third, the existence of Mo_2CT_x MXene nanoparticles in the tribofilm also provided low shear strength, which assisted in reducing friction and wear. Therefore, the COF of the boundary lubrication was very low owing to the combined action of these three principal factors.

For the elastohydrodynamic lubrication, the viscosity of Mo_2CT_x–IL increased from 1.26 to 14.36 mPa·s after the running-in period, which was beneficial for the formation of the elastohydrodynamic lubricating film. Consequently, under the synergistic effect of the boundary lubrication and elastohydrodynamic lubrication, an ultralow COF under an ultrahigh contact pressure was achieved. The results and analysis demonstrate that the introduction of Mo_2CT_x MXene additives into IL can effectively enhance the lubrication performance and suppress surface wear, which further enhances the contact pressure for superlubricity (exceeding 1 GPa). This magnitude of improvement indicates that ultrahigh load capacity and ultralow friction can be achieved simultaneously by MXene–liquid coupling lubrication. The outstanding friction performance of Mo_2CT_x MXene nanoparticles expands the feasibility of MXene materials in the field of lubrication and their potential application in the mechanical industry. Therefore, the synergistic lubrication effect between Mo_2CT_x MXene nanoparticles

and ILs has important implications for the development of the liquid lubrication with superlubricity and super-wear-resistance performance.

4 Conclusions

Robust superlubricity can be achieved using Mo_2CT_x MXene nanoparticles in combination with IL at the Si_3N_4–sapphire interface. In this study, the upper limit of the contact pressure for the liquid superlubricity state was greatly improved to 1.42 GPa at the macroscale. The formation of the composite tribofilms induced by the tribochemical reaction, mainly containing Mo_xO_y, P_xO_y, and adsorbed Mo_2CT_x MXene, suppressed the surface wear and provided an extremely low shear strength, which is the origin of the superlubricity state under ultrahigh contact pressure. This work provides a new method for achieving macroscale superlubricity under ultrahigh contact pressure through the synergistic effect of MXene and liquid molecules. The method has great potential for the application of superlubricity in mechanical systems.

Acknowledgements

This work was financially supported by the National Key R&D Program of China (No. 2020YFA0711003), the National Natural Science Foundation of China (Nos. 52005290, 51775295, and 52175174), and the Open Research Fund of Jiangsu Key Laboratory for Design and Manufacture of Micro-Nano Biomedical Instruments (No. KF202004).

Declaration of competing interest

The authors have no competing interests to declare that are relevant to the content of this article.

Electronic Supplementary Material Supplementary material is available in the online version of this article at https://doi.org/10.1007/s40544-021-0597-6.

References

[1] Luo J B, Zhou X. Superlubricitive engineering—Future industry nearly getting rid of wear and frictional energy consumption. *Friction* **8**(4): 643–665 (2020)

[2] Holmberg K, Erdemir A. Influence of tribology on global energy consumption, costs and emissions. *Friction* **5**(3): 263–284 (2017)

[3] Wang J, Zhang X W, Zhang S, Kang J Y, Guo Z C, Feng B Y, Zhao H, Luo Z, Yu J, Song W L, *et al*. Semi-convertible hydrogel enabled photoresponsive lubrication. *Matter* **4**(2): 675–687 (2021)

[4] Li H, Wang J H, Gao S, Chen Q, Peng L M, Liu K H, Wei X L. Superlubricity between MoS_2 monolayers. *Adv Mater* **29**(27): 1701474 (2017)

[5] Li J J, Gao T Y, Luo J B. Superlubricity of graphite induced by multiple transferred graphene nanoflakes. *Adv Sci* **5**(3): 1700616 (2018)

[6] Chen X C, Li J J. Superlubricity of carbon nanostructures. *Carbon* **158**: 1–23 (2020)

[7] Berman D, Erdemir A, Sumant A V. Graphene: A new emerging lubricant. *Mater Today* **17**(1): 31–42 (2014)

[8] Shi P F, Sun J H, Liu Y H, Zhang B, Zhang J Y, Chen L, Qian L M. Running-in behavior of a H-DLC/Al_2O_3 pair at the nanoscale. *Friction* **9**(6): 1464–1473 (2021)

[9] Bai C N, An L L, Zhang J, Zhang X K, Zhang B, Qiang L, Yu Y L, Zhang J Y. Superlow friction of amorphous diamond-like carbon films in humid ambient enabled by hexagonal boron nitride nanosheet wrapped carbon nanoparticles. *Chem Eng J* **402**: 126206 (2020)

[10] Gao Y, Ma L R, Liang Y, Li B H, Luo J B. Water molecules on the liquid superlubricity interfaces achieved by phosphoric acid solution. *Biosurface and Biotribology* **4**(3): 94–98 (2018)

[11] Ge X Y, Li J J, Zhang C H, Liu Y H, Luo J B. Superlubricity and antiwear properties of *in situ*-formed ionic liquids at

ceramic interfaces induced by tribochemical reactions. *ACS Appl Mater Interfaces* **11**(6): 6568–6574 (2019)

[12] De Barros Bouchet M I, Martin J M, Avila J, Kano M, Yoshida K, Tsuruda T, Bai S D, Higuchi Y, Ozawa N, Kubo M, et al. Diamond-like carbon coating under oleic acid lubrication: Evidence for graphene oxide formation in superlow friction. *Sci Reports* **7**: 46394 (2017)

[13] Martin J M, de Barros Bouchet M I, Le Mogne T, Kano M. Towards superlubricity under boundary lubrication. In *Proceedings of the World Tribology Congress III, American Society of Mechanical Engineers Digital Collection*, USA, 2005: 453–454.

[14] Arad S, Rapoport L, Moshkovich A, van Moppes D, Karpasas M, Golan R, Golan Y. Superior biolubricant from a species of red microalga. *Langmuir* **22**(17): 7313–7317 (2006)

[15] Tang G B, Su F H, Xu X, Chu P K. 2D black phosphorus dotted with silver nanoparticles: An excellent lubricant additive for tribological applications. *Chem Eng J* **392**: 123631 (2020)

[16] Liu Y F, Ge X Y, Li J J. Graphene lubrication. *Appl Mater Today* **20**: 100662 (2020)

[17] Zeng Q F, Yu F, Dong G N. Superlubricity behaviors of Si_3N_4/DLC films under PAO oil with nano boron nitride additive lubrication. *Surf Interface Anal* **45**(8): 1283–1290 (2013)

[18] Wang H D, Liu Y H, Liu W R, Liu Y M, Wang K P, Li J J, Ma T B, Eryilmaz O L, Shi Y J, Erdemir A, et al. Superlubricity of polyalkylene glycol aqueous solutions enabled by ultrathin layered double hydroxide nanosheets. *ACS Appl Mater Interfaces* **11**(22): 20249–20256 (2019)

[19] Naguib M, Kurtoglu M, Presser V, Lu J, Niu J J, Heon M, Hultman L, Gogotsi Y, Barsoum M W. Two-dimensional nanocrystals produced by exfoliation of Ti_3AlC_2. *Adv Mater* **23**(37): 4248–4253 (2011)

[20] Naguib M, Mashtalir O, Lukatskaya M R, Dyatkin B, Zhang C F, Presser V, Gogotsi Y, Barsoum M W. One-step synthesis of nanocrystalline transition metal oxides on thin sheets of disordered graphitic carbon by oxidation of MXenes. *Chem Commun* **50**(56): 7420–7423 (2014)

[21] Venkateshalu S, Grace A N. MXenes—A new class of 2D layered materials: Synthesis, properties, applications as supercapacitor electrode and beyond. *Appl Mater Today* **18**: 100509 (2020)

[22] Ghidiu M, Lukatskaya M R, Zhao M Q, Gogotsi Y, Barsoum M W. Conductive two-dimensional titanium carbide 'clay' with high volumetric capacitance. *Nature* **516**(7529): 78–81 (2014)

[23] Shen J, Liu G Z, Ji Y F, Liu Q, Cheng L, Guan K C, Zhang M C, Liu G P, Xiong J, Yang J, et al. 2D MXene nanofilms with tunable gas transport channels. *Adv Funct Mater* **28**(31): 1801511 (2018)

[24] Yi S, Li J J, Liu Y F, Ge X Y, Zhang J, Luo J B. *In-situ* formation of tribofilm with $Ti_3C_2T_x$ MXene nanoflakes triggers macroscale superlubricity. *Tribol Int* **154**: 106695 (2021)

[25] Wyatt B C, Rosenkranz A, Anasori B. 2D MXenes: Tunable mechanical and tribological properties. *Adv Mater* **33**(17): 2007973 (2021)

[26] Malaki M, Varma R S. Mechanotribological aspects of MXene-reinforced nanocomposites. *Adv Mater* **32**(38): 2003154 (2020)

[27] Rosenkranz A, Grützmacher P G, Espinoza R, Fuenzalida V M, Blanco E, Escalona N, Gracia F J, Villarroel R, Guo L C, Kang R Y, et al. Multi-layer $Ti_3C_2T_x$-nanoparticles (MXenes) as solid lubricants—Role of surface terminations and intercalated water. *Appl Surf Sci* **494**: 13–21 (2019)

[28] Yin X, Jin J, Chen X C, Rosenkranz A, Luo J B. Ultra-wear-resistant MXene-based composite coating via *in situ* formed nanostructured tribofilm. *ACS Appl Mater Interfaces* **11**(35): 32569–32576 (2019)

[29] Feng Q, Deng F K, Li K C, Dou M Y, Zou S, Huang F C. Enhancing the tribological performance of Ti_3C_2 MXene modified with tetradecylphosphonic acid. *Colloids Surf A Physicochem Eng Aspects* **625**: 126903 (2021)

[30] Lian W Q, Mai Y J, Liu C S, Zhang L Y, Li S L, Jie X H. Two-dimensional Ti_3C_2 coating as an emerging protective solid-lubricant for tribology. *Ceram Int* **44**(16): 20154–20162 (2018)

[31] Grützmacher P G, Suarez S, Tolosa A, Gachot C, Song G C, Wang B, Presser V, Mücklich F, Anasori B, Rosenkranz A. Superior wear-resistance of $Ti_3C_2T_x$ multilayer coatings. *ACS Nano* **15**(5): 8216–8224 (2021)

[32] Marian M, Feile K, Rothammer B, Bartz M, Wartzack S, Seynstahl A, Tremmel S, Krauß S, Merle B, Böhm T, et al. $Ti_3C_2T_x$ solid lubricant coatings in rolling bearings with remarkable performance beyond state-of-the-art materials. *Appl Mater Today* **25**: 101202 (2021)

[33] Guo L H, Zhang Y M, Zhang G, Wang Q H, Wang T M. MXene–Al_2O_3 synergize to reduce friction and wear on epoxy-steel contacts lubricated with ultra-low sulfur diesel. *Tribol Int* **153**: 106588 (2021)

[34] Rasheed A K, Khalid M, Mohd Nor A F B, Wong W Y, Duolikun T, Natu V, Barsoum M W, Leo B F, Zaharin H A, Ghazali M J. MXene–graphene hybrid nanoflakes as friction modifiers for outboard engine oil. *IOP Conf Ser*: *Mater Sci Eng* **834**(1): 012039 (2020)

[35] Xue M Q, Wang Z P, Yuan F, Zhang X H, Wei W, Tang H, Li C S. Preparation of TiO_2/$Ti_3C_2T_x$ hybrid nanocomposites and their tribological properties as base oil lubricant additives. *RSC Adv* **7**(8): 4312–4319 (2017)

[36] Ge X Y, Li J J, Wang H D, Zhang C H, Liu Y H, Luo J B. Macroscale superlubricity under extreme pressure enabled

by the combination of graphene-oxide nanosheets with ionic liquid. *Carbon* **151**: 76–83 (2019)
[37] Jin S, Su T C, Hu Q K, Zhou A G. Thermal conductivity and electrical transport properties of double-A-layer MAX phase Mo_2Ga_2C. *Mater Res Lett* **8**(4): 158–164 (2020)
[38] He H T, Jin S, Fan G X, Wang L B, Hu Q K, Zhou A G. Synthesis mechanisms and thermal stability of ternary carbide Mo_2Ga_2C. *Ceram Int* **44**(18): 22289–22296 (2018)
[39] Halim J, Kota S, Lukatskaya M R, Naguib M, Zhao M Q, Moon E J, Pitock J, Nanda J, May S J, Gogotsi Y, et al. Synthesis and characterization of 2D molybdenum carbide (MXene). *Adv Funct Mater* **26**(18): 3118–3127 (2016)
[40] Seh Z W, Fredrickson K D, Anasori B, Kibsgaard J, Strickler A L, Lukatskaya M R, Gogotsi Y, Jaramillo T F, Vojvodic A. Two-dimensional molybdenum carbide (MXene) as an efficient electrocatalyst for hydrogen evolution. *ACS Energy Lett* **1**(3): 589–594 (2016)
[41] Fredrickson K D, Anasori B, Seh Z W, Gogotsi Y, Vojvodic A. Effects of applied potential and water intercalation on the surface chemistry of Ti_2C and Mo_2C MXenes. *J Phys Chem C* **120**(50): 28432–28440 (2016)
[42] Byeon A, Hatter C B, Park J H, Ahn C W, Gogotsi Y, Lee J W. Molybdenum oxide/carbon composites derived from the CO_2 oxidation of Mo_2CT_x (MXene) for lithium ion battery anodes. *Electrochimica Acta* **258**: 979–987 (2017)
[43] Lee D H, Condrate Sr R A. An FTIR spectral investigation of the structural species found on alumina surfaces. *Mater Lett* **23**(4–6): 241–246 (1995)
[44] Li J J, Zhang C H, Deng M M, Luo J B, Investigation of the difference in liquid superlubricity between water- and oil-based lubricants. *RSC Adv* **5**(78): 63827–63833 (2015)
[45] Rodríguez Ripoll M, Tomala A, Gabler C, Dražić G, Pirker L, Remškar M. *In situ* tribochemical sulfurization of molybdenum oxide nanotubes. *Nanoscale* **10**(7): 3281–3290 (2018)
[46] Stolarski T A, Tobe S. The effect of spraying distance on wear resistance of molybdenum coatings. *Wear* **249**(12): 1096–1102 (2001)
[47] Nasybulin E N, Xu W, Engelhard M H, Nie Z M, Burton S D, Cosimbescu L, Gross M E, Zhang J G. Effects of electrolyte salts on the performance of Li–O_2 batteries. *J Phys Chem C* **117**(6): 2635–2645 (2013)
[48] Yi S, Chen X C, Li J J, Liu Y F, Ding S L, Luo J B. Macroscale superlubricity of Si-doped diamond-like carbon film enabled by graphene oxide as additives. *Carbon* **176**: 358–366 (2021)
[49] Guo J D, Peng R L, Du H, Shen Y B, Li Y, Li J H, Dong G N. The application of nano-MoS_2 quantum dots as liquid lubricant additive for tribological behavior improvement. *Nanomaterials* **10**(2): 200 (2020)
[50] Wang D H, Sun G D, Zhang G H. Preparation of ultrafine Mo powders via carbothermic pre-reduction of molybdenum oxide and deep reduction by hydrogen. *Int J Refract Met Hard Mater* **75**: 70–77 (2018)
[51] Wu S, He F, Xie G X, Bian Z L, Ren Y L, Liu X Y, Yang H J, Guo D, Zhang L, Wen S Z, et al. Super-slippery degraded black phosphorus/silicon dioxide interface. *ACS Appl Mater Interfaces* **12**(6): 7717–7726 (2020)
[52] Liu N, Wang J Z, Chen B B, Yan F Y. Tribochemical aspects of silicon nitride ceramic sliding against stainless steel under the lubrication of seawater. *Tribol Int* **61**: 205–213 (2013)

Shuang YI. He received his B.S. degree from Chongqing University of Technology, Chongqing, China, in 2014, and got his Ph.D. degree in mechanical engineering at Royal Melbourne Institute of Technology (RMIT), Melbourne, Australia, in 2019. He worked as a Shuimu Scholar fellowship at the Department of Mechanical Engineering, Tsinghua University, Beijing, China, from 2019 to 2021. He is currently an assistant professor at Chongqing University, Chongqing, China. His research interests are the technology of 2D material synthesis and preparation, the theory of liquid–solid lubrication, and the mechanism of superlubricity.

Yitong GUO. She received her B.S. and M.S. degrees in the School of Materials Science and Engineering, Henan Polytechnic University, China. She is currently a Ph.D. candidate with the supervision of Prof. Aiguo Zhou at Henan Polytechnic University. Her main research focuses on the properties of MAX-phases and the synthesis and applications of MXenes.

Jinjin LI. He received his B.S. degree in mechanical engineering from University of Science and Technology of China, Hefei, China, in 2009, and his Ph.D. degree in mechanical engineering from Tsinghua University, Beijing, China, in 2014. He is currently an assistant professor at Tsinghua University, Beijing, China. His major research area includes solid and liquid superlubricity, nanotribology, and friction theory. He has published more than 30 papers on the international journals (21 papers as the first author). He has been awarded the 4th Hiwin award for outstanding doctoral dissertation, first prize for outstanding doctoral dissertation, and outstanding postdoctor in Tsinghua University.

Yuxin ZHANG. He received his B.Eng. and M.Eng degrees in chemical engineering from Tianjin University, China, in 2000 and 2003, respectively. He received his Ph.D. degree in chemistry and biomolecular engineering from the National University of Singapore (NUS), Singapore, in 2008, and continued to work as a research fellow in Prof. Huachun ZENG's group at NUS until 2009. His research interests involve the preparation and application of nanomaterials, synthesis and morphology control of electrode materials in supercapacitor, and advanced design and performance research of photocatalytic materials.

Aiguo ZHOU. He received his B.S. degree from Wuhan University, China, in 1997; M.S. degree from Tsinghua University, China, in 2003; and Ph.D. degree in materials engineering from Drexel University, USA, in 2008. He joined Henan Polytechnic University in 1997. His current position is a professor, and his research area is the process and properties of layered ceramic MAX phases and 2D MXenes.

Jianbin LUO. He received his B.S. degree from Northeastern University, China, in 1982, and got his M.S. degree from Xi'an University of Architecture and Technology, China, in 1988. In 1994, he received his Ph.D. degree from Tsinghua University, Beijing, China, and then joined the faculty of Tsinghua University. Prof. Jianbin LUO is an Academician of the Chinese Academy of Sciences and a Yangtze River Scholar Distinguished Professor of Tsinghua University. He was awarded the STLE International Award (2013), the Chinese National Technology Progress Prize (2008), the Chinese National Natural Science Prize (2001), and the Chinese National Invention Prize (1996). Prof. Jianbin LUO has been engaged in the research of thin film lubrication, superlubricity, and tribology in nanomanufacturing. He was invited as a keynote or plenary speaker for more than 20 times on the international conferences.